

## Molecular Viscosity in the Normal Left Coronary Arterial Tree. Is It Related to Atherosclerosis?

Johannes V. Soulis, PhD,\* Thomas M. Farmakis, MD, PhD,  
George D. Giannoglou, MD, PhD, Ioannis S. Hatzizisis, MD, MSc,  
George A. Giannakoulas, MD, George E. Parcharidis, MD, PhD,  
and George E. Louridas, MD, PhD, *Thessaloniki and Xanthi, Greece*

The purpose of this study is to elucidate, probably for the first time, the distribution of molecular viscosity in the entire left coronary artery (LCA) tree. The governing mass, momentum, and energy flow equations were solved by using a previously validated 3-dimensional numerical (finite-element analysis) code. High-molecular-viscosity regions occur at bifurcations in regions opposite the flow dividers, which are anatomic sites predisposed for atherosclerotic development. Furthermore, high-molecular-viscosity values appear in the proximal regions of the LCA tree, where atherosclerosis frequently occurs. The effect of blood flow resistance, due to increased blood viscosity, gives rise to increased contact time between the atherogenic particles of the blood and the endothelium, probably promoting atherosclerosis. Observations suggest that, whole viscosity distribution within the coronary artery tree may represent a risk factor for the resulting atherosclerosis. This distribution can become a possible tool for the location of atherosclerotic lesions.

### Introduction

The hemodynamics within the cardiovascular system are highly influenced by mechanical factors that include blood viscosity, the pressure gradient, and local shear rates. A number of studies in the coronary arteries describe the topography of

atherosclerosis.<sup>1-3</sup> The role of blood viscosity in the development and progression of coronary heart disease (CHD) is important.<sup>4,5</sup> The influence of plasma viscosity and cellular rheology has been noticeably absent from the study of CHD. According to non-Newtonian behavior, blood viscosity is velocity gradient-dependent and subsequently varies along the course of the vessel. Henceforth, the variation is dependent on the applied flow conditions, vascular geometry, flow particularities, and local blood flow composition. Viscosity increases in bifurcations, bends, and poststenotic regions. These are the sites where blood flow is either slow or disturbed and where wall shear stresses as well as their gradients are low.<sup>6</sup> Furthermore, Junker et al<sup>7</sup> support the hypothesis that an increased plasma viscosity may be a link between cardiovascular risk factors and CHD. However, little research has focused on the

---

Angiology 57:33-40, 2006

From AHEPA University Hospital, 1st Cardiology Department, Aristotle University of Thessaloniki, Thessaloniki; and \*Fluid Mechanics, Demokriton University of Thrace, Xanthi, Greece

Correspondence: Assoc. Prof. George D. Giannoglou, 1st Cardiology Department, AHEPA University Hospital, Aristotles University of Thessaloniki, 1 S. Kyriakidi Str, 54636, Thessaloniki, Greece

E-mail: yan@med.auth.gr

©2006 Westminster Publications, Inc, 708 Glen Cove Avenue, Glen Head, NY 11545, USA

exact role of local viscosity differentiation within the coronary tree and its implications for atherogenesis.

The aims of this study are threefold: first, to compute the distribution of the non-Newtonian molecular viscosity of blood in the entire normal left coronary artery (LCA), second to quantify the differences in molecular viscosity between proximal and distal LCA parts as well as the local differences of this physical quantity in bifurcations and bends, and last, to investigate the possible implications of this distribution for the atherosclerotic lesion localization in the normal human LCA. To the best of our knowledge, there is no published computational work determining the topography of the molecular viscosity in the normal human LCA tree under resting flow conditions with atherosclerosis.

## Methods

### Geometry

Experimental measurements of the intrathoracic spatial location of specified coronary segments on the normal human heart were previously reported.<sup>8,9</sup> These studies were based on 83 angiographies in normal subjects. The intrathoracic location and course of each 1 of the 23 arterial segments and branches, which are commonly used to describe the localization of CHD, were reported. All data were processed with a computing aided design (CAD) program, resulting in a 3-dimensional geometry model of the LCA tree. To eliminate variance attributed to cardiac motion, all angiographic data corresponded to end diastole. Therefore, there was no motion incorporated in the computational fluid dynamics (CFD) calculations. The model utilized for flow analysis included the left main coronary artery (LMCA), left anterior descending (LAD), left circumflex branch (LCx), and their main branches: the first obtuse marginal (OM1), the second obtuse marginal (OM2), the first septal (S1), the first diagonal (D1), the second septal (S2), the second diagonal (D2), the third septal (S3), and the third diagonal (D3) branches. Figure 1 shows the geometry of the LCA tree as described above.

We describe the vessel centerline location (polar coordinates) and vessel diameter at each segment. In particular, the vessel centerline was constructed by using: (1) radius, (2) azimuth angle between projection of radius onto trans-

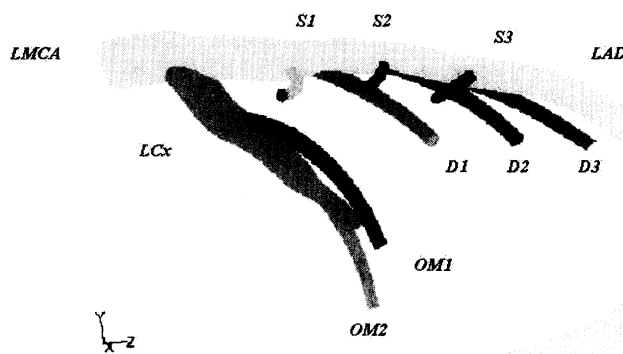


**Figure 1.** The normal left coronary artery (LCA) tree geometry includes the left main coronary artery (LMCA), left anterior descending (LAD), left circumflex branch (LCx), and their main branches: The first obtuse marginal (OM1), the second obtuse marginal (OM2), the first septal (S1), the first diagonal (D1), the second septal (S2), the second diagonal (D2), the third septal (S3), and the third diagonal (D3) branch.

verse plane and anterior-posterior axis, and, (3) angle between radius and transverse plane.

Once the vessel centerline construction was completed, the appropriate vessel diameter was applied at each segment, and the final vessel geometry was acquired via a computerized extrusion process of the preprocessing CAD program. These data were proven to be good enough to describe the anatomic location of the various anatomical segments, and the final geometry was found to be satisfactory as a model simulating the normal human left coronary anatomy.

The lumen diameter of the LMCA orifice measured 4.5 mm while the corresponding values of the LAD and LCx were 3.7 and 3.4 mm, respectively. The outlet LAD diameter at the apex of the heart measured 0.9 mm, while the corresponding diameter of the LCx at the outlet was 1.3 mm. For the first, second, and third diagonals the corresponding diameters were 1.1, 1.0, and 0.9 mm, respectively, while for the first, second, and third septals the corresponding diameters were 0.9, 0.7, and 0.7 mm. For the LCx branches, the outlet diameters of the first and second obtuse marginals were 1.1 and 1.0 mm.

### Computational Grid

All geometrical data were input into a specialized preprocessing program for grid generation.

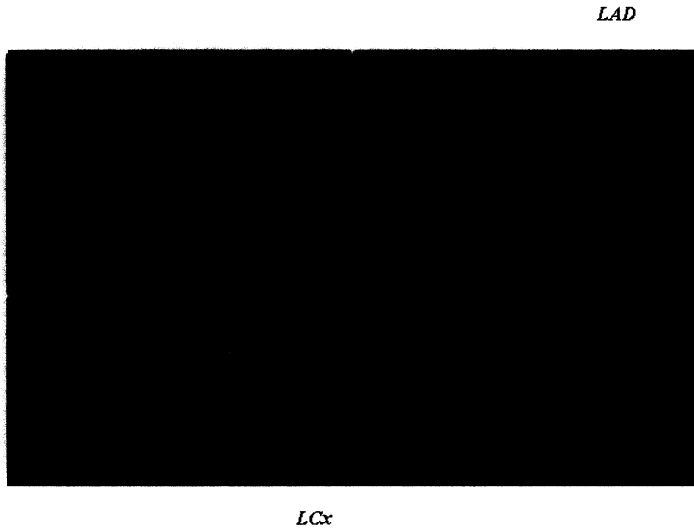


**Figure 2.** Nonstructured grid of the normal human left coronary artery (LCA) tree used for computational analysis. Details of proximal tree segments. A left main coronary artery (LMCA) plane, used for computational analysis, is also shown.

In total, 44,452 grid nodes were utilized, giving rise to a 196,902 computational tetrahedral. Figure 2 shows details of the utilized nonstructured grid of the human LCA tree. The relative error in the velocity components and in the hemodynamic parameter of wall shear stress (WSS) was computed and used as a quantitative measure of the effect of grid density. The used mesh was based on the computational results of mesh-independence studies. The number of nodes used to define the mesh independence increased initially to 59,524 nodes and at a later stage to 80,889 nodes. The relative error in the derived hemodynamic parameter of WSS was calculated

and used as a quantitative measure of the grid density effects on the results.

### Flow Equations, Boundary Flow Conditions and Solution

The blood velocity is assumed to be uniform at the orifice of the LMCA. The applied inflow conditions mimic typical coronary blood flow velocity under resting conditions, 0.17 m/s. Flow discharges were set analogous to the third power of the branching vessel diameter according to Murray's law.<sup>10</sup> Table I shows the values of the outflow flow discharges as a percentage of the inlet flow. All computational grid data, as well as all physical flow data determined from the boundary conditions, were imported into the main computational fluid dynamics solver (Fluent release 5.5, FLUENT Inc).<sup>11</sup> The numerical code, which was previously validated,<sup>12</sup> solves the governing Navier-Stokes flow equations. In the generality, these equations solve the mass, momenta, and energy conservation. The assumptions made about the nature of the flow are that it is 3-dimensional, steady, laminar, isothermal, with no external forces applied on it while the arterial wall is composed from nonelastic and impermeable material. Cardiac motion, up to 1 Hz frequency, only slightly affects the velocity changes (maximum 6%).<sup>13</sup> Therefore, the calculated results are not significantly influenced by this assumption. The governing flow equations are given in the Appendix.

### Calculated Variable

Molecular viscosity values (kg/m-s) were calculated throughout the entire LCA tree including the LMCA, LAD, LCx, and their major branches. All molecular viscosity values are shown in filled

**Table I.** Flow discharge values (%) at the outlet branches of the left coronary artery (LCA) tree (Figure 1).

| LCx   | OM1  | OM2   | S1   | D1   | S2   | D2   | S3   | D3   | LAD (Distal) |
|-------|------|-------|------|------|------|------|------|------|--------------|
| 22.44 | 5.82 | 15.42 | 2.00 | 5.49 | 1.40 | 4.72 | 3.21 | 4.20 | 35.27        |

Left circumflex branch (LCx), first obtuse marginal (OM1), second obtuse marginal (OM2), first septal (S1), first diagonal (D1), second septal (S2), second diagonal (D2), third septal (S3), third diagonal (D3) branch, left anterior descending (LAD).

contours coupled with isocontour line form. Contour labels appear in Figures 3–5, ranging from 1 to 15, and correspond to 15 color levels.

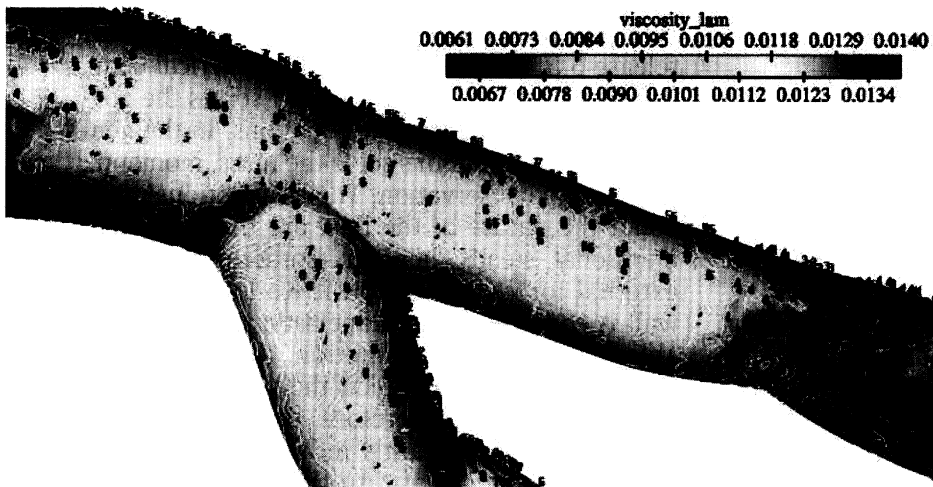
**Results**

Figure 3 shows the molecular viscosity (kg/m-s) magnitude distribution at the proximal left anterior descending (LAD) branch. These values

range from 0.0061 kg/m-s to 0.0140 kg/m-s. Figure 4 shows the contour plots of the molecular viscosity (kg/m-s) magnitude distribution at the origin of the first diagonal (D1)-first septal (S1) branches (the origin of LCx segment is also shown). Low molecular viscosity prevails at the distal LAD segment.

Figure 5 shows the molecular viscosity distribution at the exit of the computational domain referring to a typical diagonal branch (D2). Note the increased molecular viscosity values near the

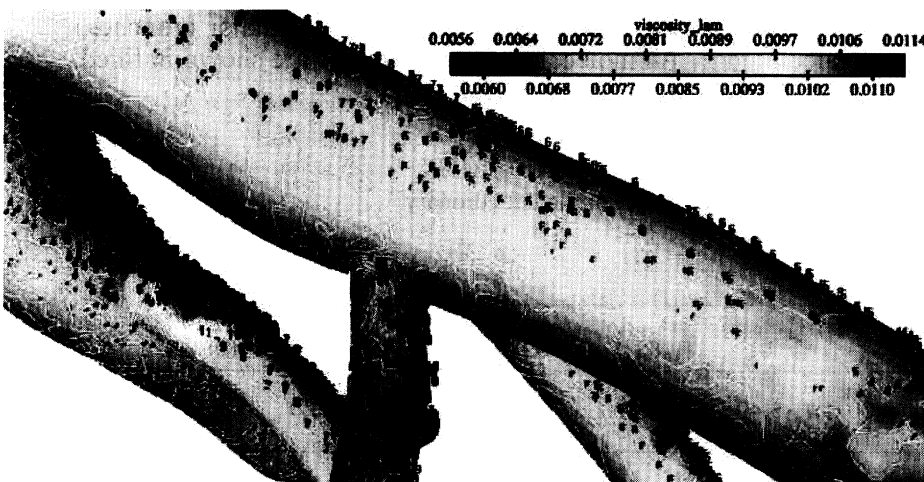
LMCA



LCx

**Figure 3.** Contour plots of the molecular viscosity (kg/m-s) magnitude distribution at the proximal left anterior descending (LAD) branch. Contour labels range from 1 to 15 and correspond to 15 color levels shown in the bar.

LAD



LCx S1

D1

LAD

**Figure 4.** Contour plots of the molecular viscosity (kg/m-s) magnitude distribution at the origin of the first diagonal (D1)-first septal (S1) branches.

center of the cross-sectional area. Viscosity values change throughout the flow field. At proximal LAD regions the near wall molecular viscosity values are of the order 0.007852 kg/m-s, while at distal LAD segments the corresponding near wall viscosity values are 0.004738 kg/m-s.

Figure 6 shows the molecular viscosity distribution at the LMCA plane (just upstream of the flow divider, also see Figure 2), while Figure 7 shows the molecular viscosity profile along the longest diameter (distance) of this plane.

## Discussion

A non-Newtonian behavior of blood in low shear regions minimizes the extent of recirculation zones.<sup>14</sup> These zones appear along a certain distance close to the arterial wall. In contrast, for Newtonian fluids, the recirculation zone extends almost into the center of the vessel cross-section. In simulating blood flow behavior certain researchers<sup>15</sup> suggest using the generalized power law model in order to achieve better approxima-

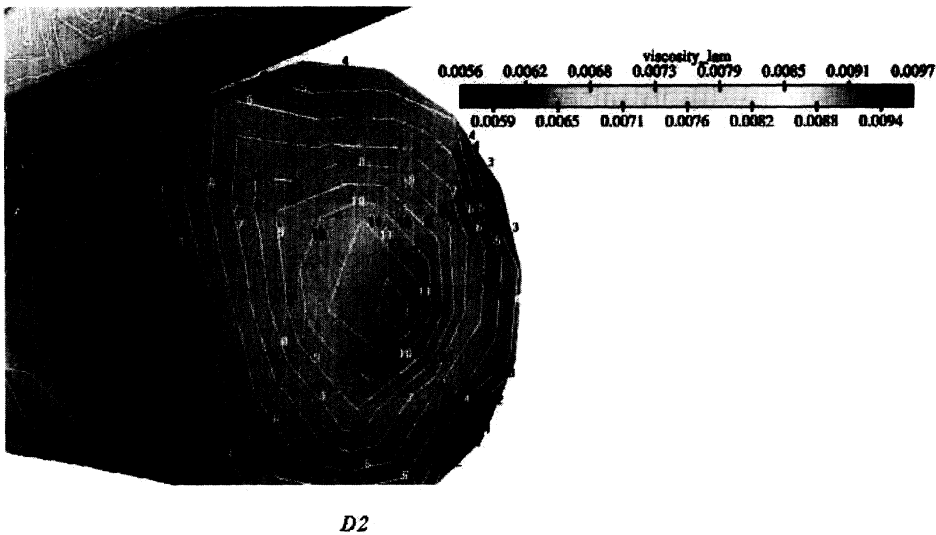


**Figure 5.** Contour plots of the molecular viscosity (kg/m-s) magnitude distribution at the exit (cross-sectional) of a typical diagonal branch (second diagonal, D2).



**Figure 6.** Contour plots of the molecular viscosity (kg/m-s) magnitude distribution at a left main coronary artery (LMCA) plane.

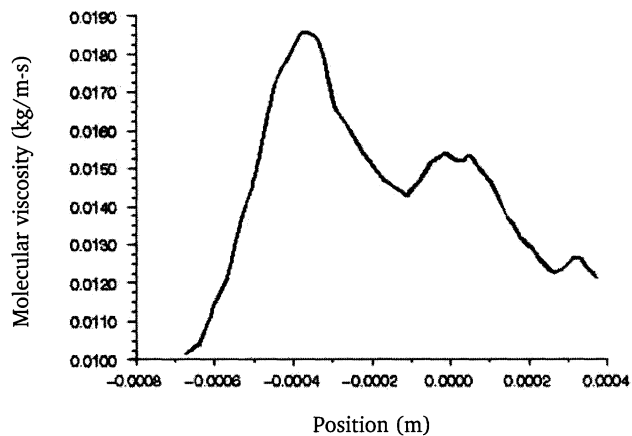


**Figure 7.** Molecular viscosity (kg/m-s) profile along the longest diameter (distance) of the left main coronary artery (LMCA) plane.

tion of wall shear stress at low shear. For atherosclerotic coronary vessels the effect of non-Newtonian viscosity of blood on hemodynamics can be more complicated than in a nondiseased vessel.<sup>5</sup> This is due to changes in local shear rate resulting from significant reductions of the cross-sectional area of the vessel segment. Plasma viscosity distribution within the coronary artery tree may represent a risk factor for the resulting atherosclerosis.<sup>16</sup> In particular, hypertension, hyperlipidemia, and diabetes increase whole blood viscosity.<sup>17</sup> It is known that, in order to maintain normal blood flow within the arterial system, the blood viscosity and the erythrocyte deformability should be adequately adapted to flow conditions.<sup>4</sup> In particular, blood viscosity must decrease while erythrocyte deformability should increase. Reduced erythrocyte deformability is of vital importance in arterial stenosed areas, resulting in an increase in both local shear rate and whole blood molecular viscosity. Moreover, increased blood viscosity in an area of plaque rupture could have a prothrombotic effect.<sup>4</sup> Therefore, the role of blood viscosity in the development and progression of CHD is very important.

Our results show that there are 3 distinct regions within the flow possessing high blood viscosity values. The first flow region, located near the center of the cross-sectional area of any segment, Figure 5, is characterized by high blood flow velocity magnitude and occupies a large section of the lumen followed by a region of reduced molecular viscosity values, extending up to the

endothelium. Figure 6 shows the locations of high-molecular-viscosity distribution regions at an LMCA plane (upstream to the flow divider). At this area there are 2 distinct high-molecular-viscosity regions corresponding to the developed flow at the entrances of the LAD and LCx segments, respectively. The highest value of the molecular viscosity distribution along the longest diameter (distance) at the LMCA plane, shown in Figure 7, is of the order of 0.0187 (kg/m-s), occurring roughly at the central region of the LAD origin. At the central region of the LCx origin, the corresponding molecular viscosity distribution value is of the order 0.0154 (kg/m-s). The exact position of these maxima values depends on the main flow pattern as it is formed in this region from the bifurcation geometry and flow conditions. Near to wall regions, the molecular viscosity values decrease, see Figures 5–7. High-molecular-viscosity values, occurring at the center region of any cross-sectional part of the LCA tree, tend to decelerate the blood flow (increased resistance).

In the second flow region (proximal–distal LCA tree), the magnitude of molecular viscosity decreases from proximal to distal flow dividers. Velocities attain large values at small size branches. These branches are frequently occurring at distal tree parts. Moreover, from the overall examination of the contours (Figures 3 and 4) it is also evident that molecular viscosity exhibits low values at distal regions of the LCA, where the magnitude of the mean flow velocity is relatively higher, owing probably to increased vessel tapering. In contrast, high-molecular-viscosity values appear at proximal LCA regions, Figure 3. This high-molecular-viscosity values distribution is in accordance with the frequent localization of atherosclerotic lesions in the proximal LCA regions. This fact further supports the possible correlation between high molecular viscosity and the localization of atherosclerosis. Given that atherosclerosis localization is less common at distal segments, compared to the proximal ones, it is also reasonable to deduce that low blood molecular viscosity has a beneficial action protecting the arterial wall.

The third flow region is located on the lateral walls of bifurcation opposite the flow divider (Figures 3 and 4), which are characterized by low wall shear stress and low velocity values. Along the vessel wall, at regions opposite to the flow dividers, where low wall shear stress and low static pressure occur, blood flow resistance effects, due to increased blood viscosity, increase the con-

tact time between the atherogenic particles in the blood and the endothelium.

Preserving molecular viscosity at low level values as well as erythrocyte deformability usually constitute physiologic adjustments in humans to maintain normal blood flow in the coronary arteries. Since viscosity is an intrinsic resistance of blood flow in vessels, the phenomenon of high viscosity regions in the central part of the lumen moderates the high blood velocity values. It is known that there is a statistically significant relation between high molecular viscosity and atherosclerosis (vessel wall thickening) of human coronary arteries.<sup>18</sup> Flow regions at the lateral walls opposite to the flow dividers are regions of high-molecular-viscosity values. A possible explanation of this phenomenon is that high-molecular-viscosity value causes low blood flow velocities, low shear rates, and consequently, low wall shear stress.<sup>18</sup> Long residence time with endothelium results in increased lipoprotein intake, and therefore, the final outcome is the thickening of the arterial vessel wall.<sup>19,20</sup>

Transport phenomena between the blood and endothelium should be further investigated. The role of blood flow on endothelium permeability must also be considered. Lipoprotein endothelium concentration should be considered as a function of local blood flow velocity, infiltration velocity at the vessel wall, and diffusion of lipoprotein molecules in blood. These would probably result in the accumulation of lipoproteins at the blood/endothelium interface. The alterations of endothelial functioning caused by molecular viscosity, wall shear stress, and wall pressure explain why the low wall shear stress in certain arterial sites favors the development of atherosclerosis. All physical factors involved in this process are characterized by a gradual and continuous change. It is obvious that the hemodynamic model describing flow must be combined with a relevant transport model for lipid accumulation into the subendothelial layer. Proper problem treatment would require the simultaneous solution of blood flow and vessel morphology partial differential equations.

## Conclusions

The influence of molecular viscosity on the normal human LCA tree was evaluated by performing a 3-dimensional computational analysis. Our

model showed a marked difference in both the magnitude and spatial distribution of molecular viscosity values in the LCA tree. This study shows that high-molecular-viscosity regions occur at bifurcations in regions opposite the flow dividers, which are anatomic sites predisposed to atherosclerotic development. High-molecular-viscosity values also appear in the proximal regions of the LCA tree, where atherosclerosis frequently occurs. At proximal LAD regions the near-wall molecular viscosity values are, approximately, double the distal segments values. The effect of blood flow resistance, due to increased blood viscosity, gives rise to increased contact time between the atherogenic particles of the blood and the endothelium, probably promoting atherosclerosis. Observations suggest that, whole viscosity distribution within the coronary artery tree may represent a risk factor for the resulting atherosclerosis. This distribution can be established as a reliable tool for predicting the location of atherosclerotic lesions.

## REFERENCES

1. Montenegro MR, Eggen DA: Topography of atherosclerosis in the coronary arteries. *Lab Invest* 18:586-593, 1998.
2. Halon DA, Sapoznikov D, Lewis BS, et al: Localization of lesions in the coronary circulation. *Am J Cardiol* 52:921-926, 1983.
3. Enos WF, Holmes RH, Beyer J: Landmark article. Coronary disease among United States soldiers killed in action in Korea. Preliminary report. By Enos WF, Holmes RH, Beyer J. *JAMA* 256:2859-2862, 1953.
4. Becker RC: The role of blood viscosity in the development and progression of coronary artery disease. *Cleve Clin J Med* 60:353-358, 1993.
5. Cho YI, Kensey KR: Effects of the non-Newtonian viscosity of blood on flows in a diseased arterial vessel. Part 1: Steady flows. *Biorheology* 28:241-262, 1991.
6. Farmakis TM, Soulis JV, Giannoglou GD, et al: Wall shear stress gradient topography in the normal left coronary arterial tree: Possible implications for atherogenesis. *Curr Med Res Opin* 20:587-596, 2004.
7. Junker R, Heinrich J, Ulbrich H, et al: Relationship between plasma viscosity and the severity of coronary heart disease. *Arterioscler Thromb Vasc Biol* 18:870-875, 1998.
8. Dodge JT Jr, Brown BG, Bolson EL, et al: Intrathoracic spatial location of specified coronary segments on the normal human heart. Applications in quantitative arteriography, assessment of regional risk and contraction, and anatomic display. *Circulation* 78:1167-1180, 1988.

9. Dodge JT Jr, Brown BG, Bolson EL, et al: Lumen diameter of normal human coronary arteries. Influence of age, sex, anatomic variation, and left ventricular hypertrophy or dilation. *Circulation* 86:232-246, 1992.
10. Murray CD: The physiological principle of minimum work. I. The vascular system and the cost of blood volume. *Proc Natl Acad Sci* 12:207-214, 1926.
11. Kelkar KM: Derivation of Pressure and Continuity Equations for FLUENT/BFC. Lebanon NH: Creare Inc, 1989.
12. Kelkar KM, Patankar SV: Development of Generalized Block Correction Procedures for the Solution of Discretized Navier-Stokes Equations. Creare Inc TM-459, Lebanon NH: Creare Inc, 1988.
13. Santamarina A, Weydahl E, Siegel J Jr, et al: Computational analysis of flow in a curved tube model of the coronary arteries: Effects of time-varying curvature. *Ann Biomed Eng* 26:944-954, 1998.
14. Liepsch D: An introduction to biofluid mechanics—basic models and applications. *J Biomech* 35:415-443, 2002.
15. Johnston BM, Johnston PR, Corney S: Non-Newtonian blood flow in human right coronary arteries: Steady state simulations. *J Biomech* 37:709-720, 2004.
16. Lowe GD, Drummond MM, Lorimer AR, et al: Relation between extent of coronary artery disease and blood viscosity. *Br Med J* 280:673-674, 1980.
17. Kensey KR, Cho YI, Chang M: Effects of whole blood viscosity on atherogenesis. *J Invasive Cardiol* 9:17-24, 1997.
18. Giannoglou GD, Soulis JV, Farmakis TM, et al: Haemodynamic factors and the important role of local low static pressure in coronary wall thickening. *Int J Cardiol* 86:27-40, 2002.
19. Asakura T, Karino T: Flow patterns and spatial distribution of atherosclerotic lesions in human coronary arteries. *Circ Res* 66:1045-1066, 1990.
20. Giannoglou GD, Soulis JV, Farmakis TM: Shear stress distribution between inner and outer right coronary artery wall at resting conditions. *Eur Heart J* 20(suppl):646, 1999 (abstract).
21. Sharma K, Bhat SV: Non-Newtonian rheology of leukemic blood and plasma: Are  $n$  and  $k$  parameters of power law model diagnostic? *Physiol Chem Phys Med NMR* 24:307-312, 1992.

---

## APPENDIX

The governing flow equations are the following:

$$\frac{\partial \rho}{\partial t} + \frac{\partial}{\partial x_i} (\rho u_i) = S_m \quad (1)$$

where  $\rho$  (kg/m<sup>3</sup>) is the density,  $t$  (sec) is the time,  $u_i$  (m/s) are the velocity components along the  $x_i$ , (m) axes,  $S_m$  is the added or subtracted mass of fluid in the flow field. The conservation of momentum along the  $i$  direction is written,

$$\frac{\partial \rho}{\partial t} (\rho u_i) + \frac{\partial}{\partial x_j} (\rho u_i u_j) = -\frac{\partial \rho}{\partial x_i} + \frac{\partial \tau_{ij}}{\partial x_j} \rho g_i + F_i \quad (2)$$

Here,  $\rho$  (N/m<sup>2</sup>) is the static pressure,  $\tau_{ij}$  (N/m<sup>2</sup>) is the shear stress tensor,  $\rho g_i$  (N/m<sup>3</sup>) and  $F_i$  (N/m<sup>3</sup>) is gravity and externally acting forces, respectively. The blood was considered to be non-Newtonian fluid obeying to the power law.<sup>21</sup> According to this law the fluid shear stress, denoted by  $\tau$  (N/m<sup>2</sup>), is calculated as,

$$\tau = [\eta(\dot{S})] \dot{S} \quad \eta(\dot{S}) = k e^{\frac{T_0}{T}} \dot{S}^{n-1} \quad \dot{S} = \frac{\partial u_i}{\partial x_j} + \frac{\partial u_j}{\partial x_i} \quad (3)$$

the consistency index  $k$  equals to 0.01691 (kg-s<sup>n-2</sup>/m), the power-law index  $n$  equals to 0.7, while  $T$  (K) and  $T_0$  (K) are local temperature and reference temperature, respectively.<sup>21</sup>